JGR Space Physics

RESEARCH ARTICLE
10.1029/2019JA027360

Observation of Very Short Period Atmospheric Gravity Waves in the Lower Ionosphere Using Very Low Frequency Waves

Ajeet K. Maurya[1], Morris B. Cohen[2], Kondapalli Niranjan Kumar[3], D.V. Phanikumar[4], Rajesh Singh[5], P.K. Vineeth[6], and K. Kishore Kumar[7]

[1]Department of Physics, Doon University, Dehradun, India, [2]School of Electrical and Computer Engineering, Georgia Institute of Technology, Atlanta, GA, USA, [3]Physical Research Laboratory, Ahmedabad, India, [4]Aryabhatta Research Institute of Observational Sciences, Nainital, India, [5]Dr. K S K Geomagnetic Research Laboratory, Indian Institute Geomagnetism, Allahabad, India, [6]Masdar Institute, Khalifa University, Abu Dhabi, UAE, [7]Vikram Sarabhai Space Center, Space Physics Laboratory, Trivandrum, India

Key Points:
- Very short period wavy fluctuations recorded in the VLF signals and are connected with the convective storms in the troposphere
- Similar very short period wavy fluctuations are also noted in GPS TEC data
- The present results provide evidence for dynamical coupling between troposphere and ionosphere through short period AGWs

Correspondence to:
A. K. Maurya,
ajeet.iig@gmail.com

Citation:
Maurya, A. K., Cohen, M. B., Niranjan Kumar, K., Phanikumar, D. V., Singh, R., Vineeth, P. K., & Kishore Kumar, K. (2019). Observation of very short period atmospheric gravity waves in the lower ionosphere using very low frequency waves. *Journal of Geophysical Research: Space Physics*, *124*, 9448–9461. https://doi.org/10.1029/2019JA027360

Received 31 AUG 2019
Accepted 19 OCT 2019
Accepted article online 25 OCT 2019
Published online 14 NOV 2019

Abstract We present observations of very short period (<5 min) wavy fluctuations (WFs) in the lower ionosphere (75–85 km) on the night of 21 January 2016, using subionospherically propagating very low frequency signals. Four out of six transmitter signals recorded by the very low frequency/low frequency receiver at the Pisgah Astronomical Research Institute showed WFs simultaneously. However, their time of occurrence and intensities were different. Power spectral analysis indicates a period of ~3–4 mins, largely associated with the two regions of strong convective and lightning activity in the lower troposphere. Background wind (at ~15 and 80 km) direction shows westward propagation, suggesting important role of the convective storm located east of Pisgah Astronomical Research Institute. The GPS total electron content analysis also divulges similar WFs at upper ionospheric altitude (~300 km) on the GPS total electron content stations around the two storms. The observational analysis suggests atmospheric gravity waves from the convective regions propagate upward up into the ionospheric altitudes. Hence, the present study reinforces the strong coupling of troposphere and ionosphere through the convectively generated very short period waves.

1. Introduction

It is known that atmospheric gravity waves (AGWs) play a vital role in shaping the structure and dynamics of the lower, middle, and upper atmosphere (Fritts & Alexander, 2003; Hines, 1960; Jones et al., 1997). Short period (<5 min) gravity waves with large horizontal phase speeds reach higher altitudes without being filtered by the background winds and have potential to transfer large amount of energy and momentum to the upper atmosphere, thus influencing the local dynamics (Garcia & Solomon, 1985; Hines, 1960; Miller et al., 2015; Nina & Čadež, 2013; Niranjan Kumar et al., 2012). The major sources of AGWs include the dynamical and convective instabilities caused by large wind shears and moist convection in the troposphere, atmospheric frontal systems, topography, earthquakes, volcanic eruptions, solar eclipse, and geomagnetic disturbances (e.g., Alexander & Teitelbaum, 2007, 2011; Durran, 1986; John & Kumar, 2013; Kumar, 2006; Niranjan Kumar et al., 2012).

Earlier studies have emphatically shown that the gravity waves undergo viscous dissipation, saturation, wave breaking, and critical level filtering in the mesosphere, and as a result, only a very small fraction of these waves reach the ionosphere (John & Kumar, 2013; Miller et al., 2015). On the other hand, the acoustic branch of high-frequency gravity waves (periods less the Brunt-Vaisala periods), owing to their higher horizontal phase speeds, can propagate to higher altitudes in the ionosphere and influence the upper atmospheric dynamics (Kherani et al., 2009; Miller et al., 2015; Nina & Čadež, 2013). Nishioka et al. (2013) reported the observations of both acoustic and gravity waves which persisted for almost few hours in the ionosphere. These waves generated due to the convection caused by the tornado in the Oklahoma state of the United States. The passage of the solar terminator during sunset and sunrise hours is also known to have triggered both acoustic and gravity waves (Nina & Čadež, 2013). There exists a considerable amount of observational evidences for acoustic/gravity waves excitation during the earthquake events (e.g., Matsumura et al., 2012). Several observational evidences are also evident of acoustic wave showing the gravity waves

signatures which was also supported by different modeling and numerical simulation groups around the globe. Sinvely (2017) in the numerical simulation work showed that the short period (~4–8 min) gravity waves in the mesosphere and lower thermosphere may produce secondary acoustic waves of ~2–4-min period, which can reach up to ionospheric altitudes. Vadas (2013) showed observations of acoustic and gravity waves from simulated convective plumes. Snively (2013) in their modeling work depicted the acoustic and gravity waves generated simultaneously by transient updrafts. A variety of experimental techniques such as radar, lidar, and rocket sonde are used to investigate the myriad manifestation of gravity waves in the upper atmosphere, but all these methods provide very limited information because of their high cost of operation, limited coverage of geographical region, and limited timing.

Some recent reports have studied the lower ionosphere/D-region during geomagnetically quiet days and during geophysical events by utilizing the very low frequency (VLF, 3–30 kHz) data sets (Maurya et al., 2012b, 2014). Maurya et al. (2012b) developed a method to estimate D-region electron density based on the lightning generated tweek radio atmospherics, whereas Maurya et al. (2014) used VLF signal from various transmitters and studied properties of AGWs observed at D-region altitude during solar eclipse conditions. The advantage to VLF waves is that they reflect efficiently from the lower ionosphere (60–90-km altitude) and are thus highly sensitive to even small changes in the electrical properties at these altitudes. Moreover, VLF waves travel to global distances, so a single path link from a transmitter to a receiver provides a diagnostic tool over an entire area.

There have been few observational reports of AGWs, as they have periods less than Brunt-Vaisala in the ionosphere. A very high temporal sampling of the geophysical parameters is a prerequisite for characterizing these waves, which makes VLF remote sensing a useful tool for investigating such high-frequency AGWs in the lower ionosphere (Nina & Čadež, 2013). AGWs affect D-region parameters when they propagate to these altitudes causing discontinuity/irregularities/gradients in different parameters such as temperature, conductivity, electron density, etc., which in turn affect VLF waves, propagating via multiple reflections through D-region. Thus, the imprint of AGWs should be clearly seen in VLF signal, and their analysis provides emphatic information about the morphology of AGWs (Maurya et al., 2014; Nina & Čadež, 2013). Nina and Čadež (2013) reported the observations of AGWs, due to the passing of solar terminator using VLF transmitter signals. The solar terminator triggers wide range of waves, including acoustic-gravity waves (period ~60–400 sec) and gravity waves (~300–400 sec; ~1,000–3,000 sec). Another interesting observation of the rare short period wave fluctuations (WFs) using VLF signals was reported by Marshall and Snively (2014). They found that the observed WFs are coherent acoustic gravity waves with a period between ~60 and 240 sec (~1–4 min). They suggested that the waves were generated due to the lightning and convective regions located directly below the transmitter-receiver great circle paths (TRGCPs) of NAU VLF transmitter signal recorded at five stations. Further at the upper ionospheric altitude, Lay et al. (2013) presented 2–4-min WFs in the differential vertical total electron content (DVTEC) data derived from several GPS stations around thunderstorm/lightning activity regions. They have reported anomalous DVTEC variations (WFs) closely associated with the underlying thunderstorms.

In this study, we show, for the first time, very short period gravity wave signatures also called as wavy fluctuations (WFs) on the four VLF transmitter signals recorded at one receiving station. The most probable source for these high-frequency waves may be lower atmospheric convective/lightning activity located away from the TRGCPs. The VLF signal passing directly above the thunderstorm, however, shows very small wave activity. In this study, we address the following important scientific questions: What are the sources and background conditions (location, size, and background wind direction) for the generation of short period WFs? Can these waves from a thunderstorm propagate to the lower and upper ionosphere? What is the role of these waves in the thermospheric-ionospheric coupling process?

2. Recording Setup and Data

The VLF data are continuously recorded using the Atmospheric Weather Electromagnetic System for observation Modeling and Education (AWESOME) (low-frequency receiver) built at Georgia Tech (Cohen et al., 2018). An earlier VLF version of the AWESOME receiver was developed at Stanford University (Cohen et al., 2010). The receiver consists of two orthogonal loop antennas to pick the horizontal component of magnetic field density from north to south and east to west vertical planes. Data are sampled at 1 MHz using a 16-bit

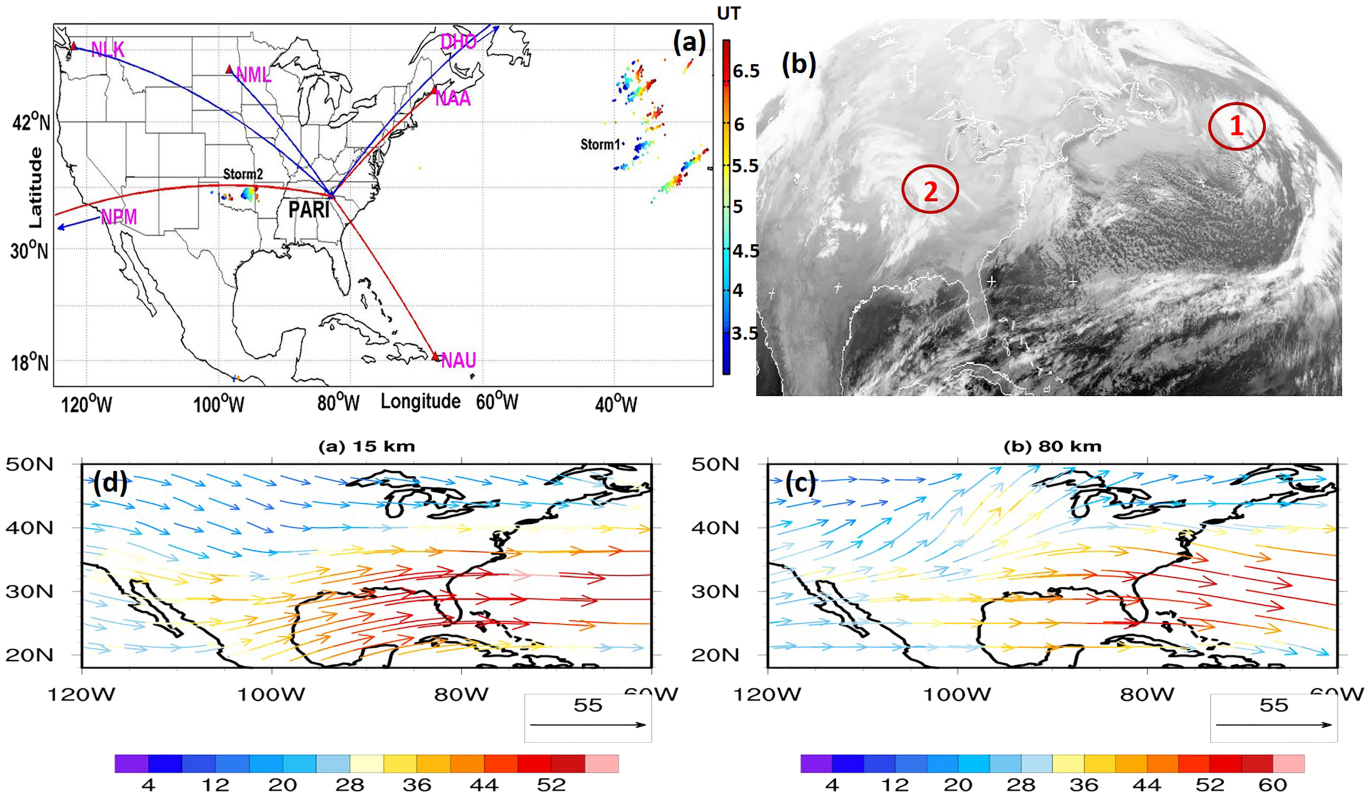

Figure 1. **(a)** Map showing location of very low frequency/low frequency recording station Pisgah Astronomical Research Institute (PARI) and six transmitters along with two lightning storm regions. The lightning activity is also shown as time color code. **(b)** The GOES13 infrared image at 05 Universal Time, showing cloud cover at two regions (marked 1 and 2) of strong conventions. **(c)** and **(d)**, respectively, showing westward winds from European Centre for Medium-Range Weather Forecasts Reanalysis 5 wind data at 80- and 15-km altitudes. Colorbar signifies the magnitude of vector wind (indicated by wind vectors of different colors), while the arrow indicates the reference vector indicating the vector wind magnitude for that length of vector.

Analog to Digital Converter. The receiver uses GPS for time synchronization with <20-ns accuracy. The data are digitized with 16-bit dynamic range. The receiver is capable of recording broadband (baseband) signals and demodulating narrowband VLF transmitters to extract amplitude and phase. The receiver is calibrated by injecting a known signal into the preamplifier. Figure 1a shows the geographical locations of VLF/LF transmitters and receiver used in the present study. Six VLF/LF transmitter signals recorded at the Pisgah Astronomical Research Institute (PARI) which hosts a VLF/LF receiver (Geog. Lat. 35.20 N, Geog. Long. 82.87 W). The transmitter and receiver details are also presented in Table 1.

We have observed very short period WFs on four transmitter signals, namely, NAA, NAU, NML, and NPM. Lightning data are obtained from Vaisala Inc's ground-based global lightning detection (GLD360) network which uses the radiated VLF energy from lightning strokes to determine the time, location, discharge polarity, and radiated peak current of lightning strikes. GLD360 has a detection efficiency of ~70%. Median geolocation accuracy of GLD360 is 1–4 km for cloud-to-ground strokes (Said et al., 2010; Said et al., 2013). GLD360 data can be obtained by contacting Vaisala Inc. for scientific purposes. Lightning strokes reported by GLD360 are shown in the top left panel of Figure 1. The colorbar indicates the time of the stroke, as reflected in each dot, so that the time evolution of lightning activity can be seen. The two strong lightning active regions are visible and marked as Storm 1 and Storm 2, respectively. Storm 1 is stronger and covers a larger region than Storm 2.

The top right panel of Figure 1 shows the convective storm, as revealed with GOES 13 mid infrared (IR) images (range 3.8–4.0 μm) at 05 Universal Time (UT). The images can be directly downloaded using the link (http://www.sat.dundee.ac.uk/). Background wind data are shown in the bottom two panels of Figure 1. We use wind data from the European Centre for Medium-Range Weather Forecasts (ECMWF) Reanalysis 5 product. The ECMWF Reanalysis 5 data are one of the advanced reanalysis data set from European Centre for

Table 1
Shows the Six Very Low Frequency Transmitters Recorded With Their Operating Frequency and Locations

VLF transmitter	Latitude	Longitude	TRGCP path length (km)	Periodicity (duration UT hours)	Peak to peak amplitude (dB)
NAA (24 kHz)	44.64 N	67.28 W	1,689	~204 sec (4:50–07 UT)	0.7
NML (25.2 kHz)	46.36 N	98.33 W	1,792	~195 (5:10–6:20 UT)	0.5
NPM (21.4 kHz)	21.4 N	158.12 W	7,257	~164 (5:30–6:30 UT)	0.15
NAU (40.8 kHz)	18.39 N	67.17 W	2,426	~174 (5:10–6:20 UT)	0.3
DHO (23.4 kHz)	53.07 N	7.61 W	6,020	Not present	
NLK (24.8 kHz)	48.20 N	121.91 W	3,501	Not present	

Note. The details on WFs duration and peak to peak amplitude also shown. TRGCP = transmitter-receiver great circle path; VLF = very low frequency.

Medium-Range Weather Forecasts with several improvements used for the generation of the product relative to earlier versions including use of Hadley Centre Global Sea Ice and Sea Surface Temperature. Two data set, new radiative transfer scheme, improve historical records of climate data and also several bias corrections related to data assimilation (ECMWF, 2017). The data are produced in 137 hybrid sigma-pressure levels covering surface to ~80-km altitude, with spatial resolution of ~31 km (Malardel et al., 2015). Both the data Hadley Centre Global Sea Ice and Sea Surface Temperature (http://www.metoffice.gov.uk/hadobs/hadisst/) and ECMWF (https://apps.ecmwf.int/datasets/) can be downloaded. The two panels reflect the winds at 15- (left) and 80-km (right) altitude. These reference levels are chosen to correspond to cloud altitude and nighttime VLF reflection height, respectively.

3. Observations

3.1. VLF Observations

Figures 2a and 2b depict the diurnal amplitude and phase variations of the six VLF transmitters signals received at PARI recording station on 21 January 2016. The WFs in both amplitude and phase are shown in the zoomed portion of 2-hr duration (during 04:30–06:30 UT) of the six transmitter signals in Figures 2a and 2b. It can be clearly seen in Figures 2a and 2b that the WFs were dominant only in four transmitter signals, namely, NAA, NAU, NML, and NPM. Further, the occurrence time and amplitude of WFs are also different, and more details are presented in Table 1. This is not unexpected, as each transmitter-receiver path samples a different portion of the ionosphere. The WFs on the NPM signals are relatively weaker due to lower SNR. Moreover, the spikes are the manifestation of lightning generated sferics due to thunderstorm below the TRGCPs (Maurya et al., 2012a). The other two transmitters, DHO and NLK, do not show any signatures of WFs. WFs are seen in both amplitude and phase of VLF signals. But in this work, we have used only amplitude data due to easy analysis compared to phase data.

In order to bring out the spectral features of the WFs, we have applied power spectral analysis technique as illustrated in Figure 3. Figure 3a (left panel) shows the Fast Fourier Transform (FFT) of the NAA transmitter signal amplitude between 4:30–6:30 UT, which exhibits dominant period of 200 sec. The FFT for other three transmitters NAU, NML, and NPM is shown in Figures 3b, 3c and 3d (left panel). The dominant period found in these transmitters is presented in Table 1, which varies between ~170 and 200 sec, all of which are substantially less than the Brunt-Vaisala period at those heights (~300 seconds). Further, we have used Butterworth digital band pass (BBP) filter to filter VLF signal amplitude for the range of 120–300-sec (~2–5 min) duration. This duration is chosen to cover dominant periods found in the FFT analysis of the VLF transmitter signal amplitude. The BBP filter amplifies the selected band range and reduces both the high and low periods. Butterworth filters have a magnitude response that is maximally flat in the passband and monotonic overall. The more details on the BBP filter can be found in Butterworth (1930). The BBP filter applied to the four transmitters signals (NAA, NAU, NML, and NPM), and the results are depicted in Figures 3a–3d (right panel).

3.2. GPS TEC Observations

The GPS TEC analysis is also carried out to show the coupling between lower ionosphere and upper ionosphere. The GPS TEC measurements are obtained from several GPS receiving stations from the

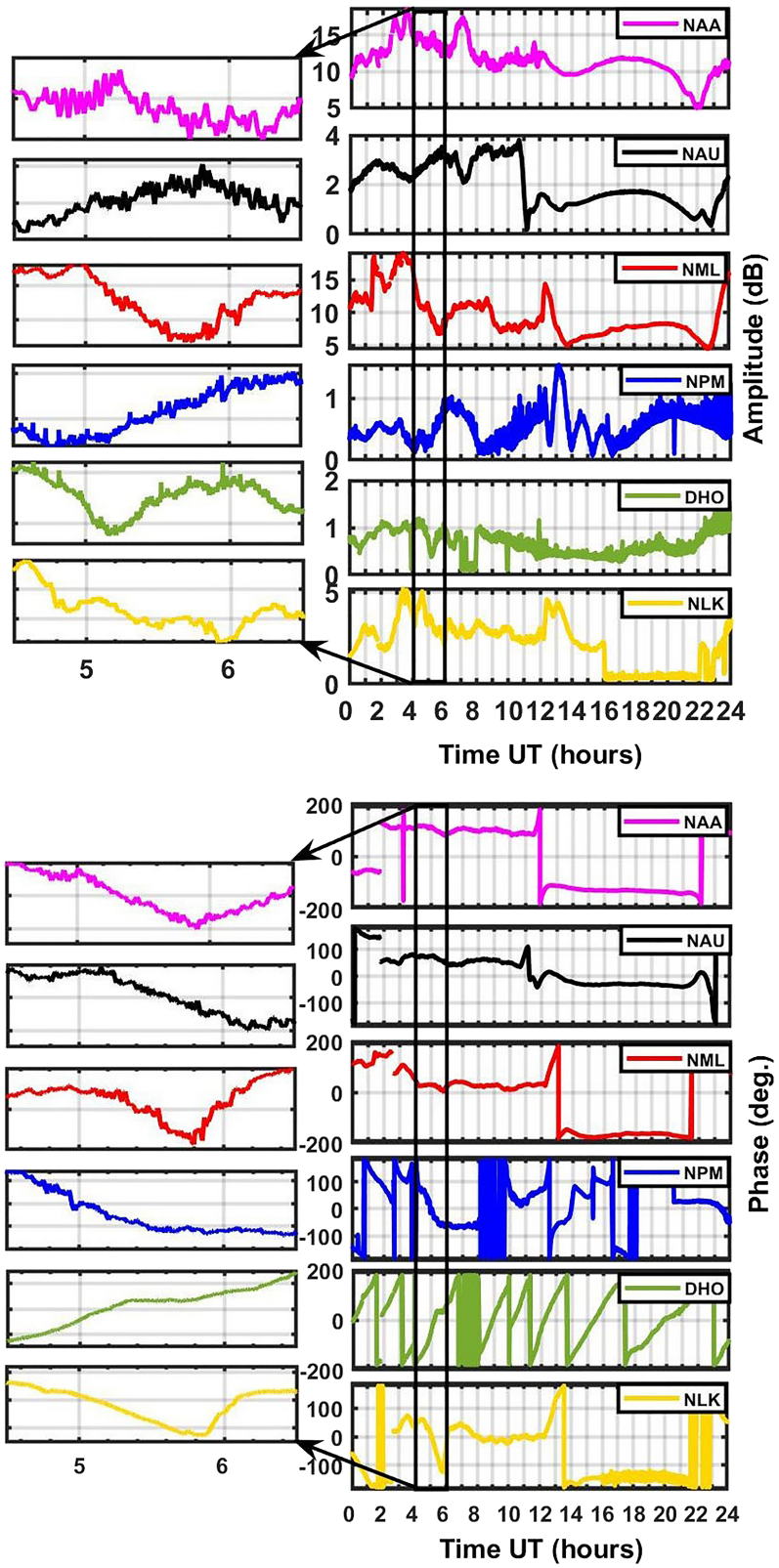

Figure 2. **(a)** (right panel) shows amplitude variation on 21 January 2016 for six transmitter signals (NAA, NAU, NML, NPM, DHO, and NLK) recorded at Pisgah Astronomical Research Institute receiving station. **(a)** (left) panel shows the zoomed portion of very low frequency amplitude between 4:50 and 6:30 Universal Time, showing wavy fluctuations on four transmitter signals (NAA, NAU, NML, and NPM). (b) The right and left panels showing phase variation similar to **(a)** right and left panels.

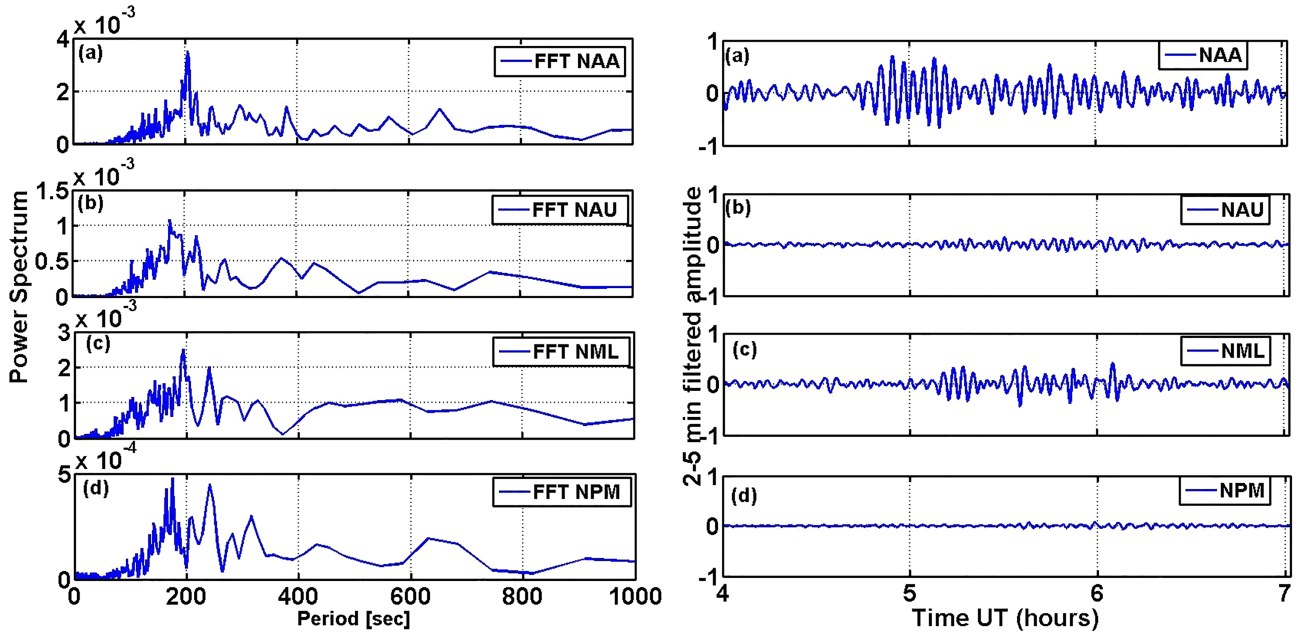

Figure 3. (a–d). (left panel) Fast Fourier transform of NAA, NAU, NML, and NPM amplitude, respectively, during 4–7 Universal Time, which depicts peak at ~207 (~3.5 min), ~194, ~164, and ~174 sec, respectively. (Figures 3a–**3d right panel)** 2–5 min filtered amplitude of NAA, NAU, NML, and NPM transmitters signal, respectively.

Continuously Operating Reference Station (http://geodesy.noaa.gov/CORS/) network during 21 January 2016. TEC is an excellent diagnostic tool of the upper ionosphere electron density, which is physically distinct from the lower ionosphere electron density. However, AGWs that reaches the lower ionosphere may also have an impact on the upper ionosphere, thus making GPS TEC a very useful comparative measurement. A subset of GPS stations within CORS is selected based on their location along the TRGCPs of six transmitters with PARI receiving station, to cover the large geographical regions around the two storms and data availability. The GPS TEC analysis provides vertical total electron content (VTEC) from the slant TEC (STEC) as reported by researchers in the past (Ramarao et al., 2006; Seemala & Valladares, 2011).

We have chosen a suitable satellite pseudo random number 30 passes, due to its coverage for the duration of 3–7 UT. Further, we have estimated differential VTEC (DVTEC) by fitting a ninth order polynomial to the VTEC data for each station as described in earlier studies (e.g., Lay et al., 2013; Ozeki & Heki, 2010). This method is effective in removing the long periodic variations if any, and the results are illustrated in Figure 4. Figure 4a indicates the details of GPS stations analyzed in this work along with the two circles representing two rough regions of influence corresponding to two thunderstorms. The GPS stations in the Region 1 are assumed to be roughly influenced by Storm 1, while stations in the Region 2 are influenced by Storm 2. The estimated DVTEC results for both regions are presented in Figures 4b and 4c. Figure 4b shows the DVTEC variation for the GPS stations under Region 1 (marked by the circle) which show wave signatures in several stations. These WFs and corresponding GPS stations are marked with red colors in Figures 4a and 4b. The WFs are seen in the GPS stations under Region 1 and are roughly located along the NAA, DHO, NAU, and NML TRGCPs, and at first instance it may be assumed that they are affected due to the AGWs generated from convective activities at Storm 1. For the Region 2, strong fluctuations are seen for the stations close but south of the Storm 2. These GPS stations are marked in magenta color in Figure 4a (Region 2). The corresponding DVTEC fluctuations are marked in red color in Figure 4c. The relatively smaller fluctuations are also evident at the stations below the NPM-PARI TRGCP. As these stations are very close to Storm 2, hence, these are most probably influenced by the convection activity of Storm 2. Also, the fluctuations in DVTEC are seen only at stations located in south of the Storm 2, except two station very close to north of Storm 2. Therefore, it is most probable that DVTEC fluctuations observed at the stations under Region 1 are affected by the convection activity at Storm 1. An example of DVTEC variation for

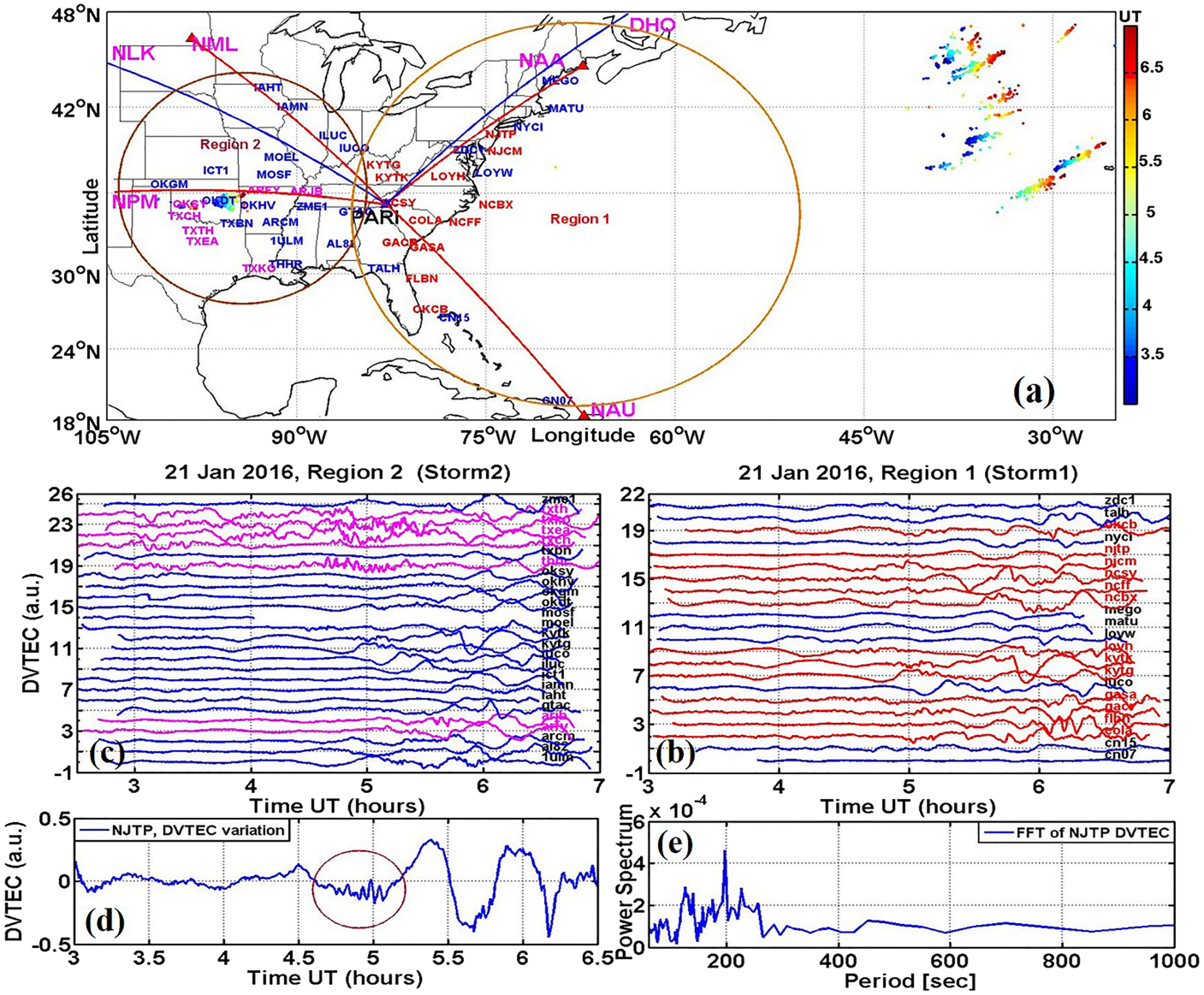

Figure 4. **(a)** Depicts the locations of GPS stations around the two storms, very low frequency/low frequency transmitter-receiver great circle paths with recording station PARI and time coded two lightning storm regions. The two circle drawn are representing the GPS stations under Region 1 and Region 2, corresponding to Storms 1 and 2, respectively. (**b)** DTEC variation for the stations under Region 1, red color lines showing WFs possibly due to Storm 1. (**c)** GPS stations under Region 2, the magenta color lines showing WFs possibly due to Storm 2. (**d)** The DVTC variation of NJTP GPS station along with WFs seen within the circle (**e)**The Fast Fourier Transform (FFT) of differential vertical total electron content data for GPS station NJTP.

NJTP GPS station located close to the mid of PARI-NAA TRGCP is shown in Figure 4d, along with the WFs marked by the circle. Further, dominant periodicities in the NJTP DVTEC data are around ~200 sec as evident from Fourier analysis, which again in the range of AGW periods observed in the VLF signals.

4. Discussion

4.1. AGWs in Lower Ionosphere

The Marshall and Snively (2014) presented first detailed work on the observation of short period (<5 min) WFs on the VLF transmitter signals. The present work provides further advancement in our understanding of the short period waves at lower and upper ionosphere. Though both works report similar observations of short period wave using VLF waves, the key difference between the two is as follows: The Marshall and

Table 2
Showing Magnitude of Background Level and Wavy Fluctuations Amplitude of Four Transmitter Signals and Start Time of WFs

VLF transmitter	Background amp	Wavy amp	Start time
NAA	0.056	0.16	~04:43 UT
NAU	−0.048	−0.084	~05:10 UT
NML	−0.104	−0.200	~05:09 UT
NPM	−0.019	−0.054	~05:36 UT

Snively (2014) observed one transmitter signal at different recording stations, with all TRGPCs passing directly above the thunderstorm. In present case, we have one receiving station recording VLF signal from several different transmitters covering very large geographical area. The implication is that we are detecting AGWs not over the thunderstorm, but actually far away in different directions from the thunderstorm after the AGWs have propagated a significant distance. We were able to detect AGWs at a distance from the thunderstorm, apart from this we are also able to determine direction of AGWs by observing start time of AGWs in different TRGCPs.

Clearly, the present study demonstrates that the VLF radio wave signal is modulated by a perturbation in the lower ionosphere (75–85-km altitude), triggered by a propagating neutral density wave, possibly an acoustic gravity wave (Figures 2, 3, and 4). Numerous sources for exciting acoustic gravity waves are reported in earlier studies which include earthquakes, solar eclipse, volcanic eruption, geomagnetic storms, solar terminator, and thunderstorms (Kherani et al., 2009). We can rule out earthquake, solar eclipse, and volcanic eruptions as there were no such events reported nearby. Examination of the geomagnetic activity shows only moderate activity, and the Kp values were@ 4-, 6-, Dst was -38 to -37 nT during 4–5 UT on 21 January 2016. This moderate activity has a negligible effect on the lower ionosphere especially at the VLF reflection height (~75–80-km altitude) (Kumar & Kumar, 2014; Peter et al., 2006). This event also occurred during 4–7 UT (local time in the region), so we can rule out any effect of the solar terminator.

We do, however, observe a strong convection storm followed by intense lighting activity during the observational period which could possibly be a potential trigger for generating AGWs. As shown in the Figure 1b, the GOES IR images show cloud coverage over the region. There we marked two brown circles as 1 and 2, which correspond to the two lightning activity region of Storm 1 and Storm 2, respectively. The Region 1 and Region 2 are the sources of strong convection and may be plausible source for the observed AGWs. However, still the generation mechanism of such a short period gravity waves is not clearly understood yet. Region 1 appears to be stronger (as per the satellite image) but located farther from PARI than Region 2. However, both the storms have a large amount of lightning activity in the presence of convective clouds.

Less clear, however, is which storm (if not both) was responsible for the WFs observed in the VLF signals. The timing and amplitude of WFs observed in the Figures 3a–3d (right panel) provide valuable information on the arrival direction of WFs from the source. We have used the following method to estimate arrival time/start time of WFs in each transmitter signal. The start time of WFs is estimated based on their appearance in the Figures 3a–3d (right panel). First, we have estimated background filtered amplitude of each transmitter signal in Figures 3a–3d (right panel), then the arrival time of WFs is defined as the time when amplitude is almost double of the background value. The detail results are presented in Table 2. As seen in Table 2, WFs first appeared on the NAA transmitter signal and then at the nearly same time on NML and NAU and later at NPM. This indicates that source may be located east of NAA-PARI TRGCP and AGWs from source propagating toward west, arriving at NAA-PARI transmitter first. As the AGWs are propagating toward west, their intensity decreases. This is supported by the fact that WFs have the strongest amplitudes for NAA received signals. As per the geographic location of NML and NAU transmitter, NAU transmitter is located closer to Storm 1. Therefore, WFs must have been appeared first at NAU with stronger amplitude compare to NML if we assume uniform velocity and intensity/strength of AGWs while traveling toward west and southwest from Storm 1. But as the WFs are stronger at NML compared to NAU and appears at nearly same time on both signals, therefore, our assumption of uniform velocity and intensity/strength of AGWs toward west and southwest is not correct and might be depends on the background wind (Nishioka et al., 2013). Interestingly, no dominant WFs were observed for DHO and NLK transmitter signals. For DHO transmitter possibly due to very long TRGCP (~6000 km), or due to weak amplitude (~1 dB) compared to NAA (~15 dB), AGWs do not show significant effect. For NLK transmitter, possibly AGWs after crossing NML-PARI TRGCPs get attenuated and do not affect NLK-PARI TRGCP. The very small WFs seen in the NPM signal may be associated with AGWs due to Storm 2. It is also possible that Storm 2 has produced very weak AGWs; hence, they affected the very closest TRGCP (NPM) and get attenuated as they move further.

Therefore, observations suggest that either storm (Storm 1 or 2) is a plausible source of the observed AGWs. Here, it should be noted that the previous works have suggested various processes that can generate observed WFs from thunderstorms. The convective plum model (when convective thunderstorm activity overshoots the tropopause) is one of the important mechanisms suggested by several works in the recent past (e.g., Alexander et al., 1995; Vadas & Liu, 2009). Vadas and Liu (2009) observed gravity waves generated by deep convective plum in thunderstorm. These AGWs propagate upward opposite to background wind direction and dissipate at thermosphere and ionosphere altitude ~120–250 km. Piani et al. (2000) in their 3-D numerical models of tropospheric convection associated with thunderstorm, confirm that the spatially isolated systems produce gravity waves. The other mechanisms are the charge and current associated with thunderstorm, and direct coupling of thunderstorm-generated electric field through ExB drift may generate WFs in the ionosphere (Sentman et al., 2003; Kuo & Lee, 2015). The thunderstorm-associated current may directly interact with lower ionosphere and cause the transient luminous event (TLEs). The TLEs are also found to be associated with observation of AGWs (Sentman et al., 2003). The electrical effects from the thunderstorm can cause ExB plasma drift motion and perturbed TEC (Kuo & Lee, 2015). As in the present case, we do not have any observations of TLEs event or the ExB drift; therefore, the most possible mechanism is the convection. Further, it is also possible that more than one mechanism may be operating simultaneously leading to even more complex mechanism. Therefore, more modeling and data analysis efforts are needed in the future to understand the possible mechanisms associated with the observed perturbations.

As seen from Figures 1c and 1d, the wind direction during the observational period shows mostly westerlies throughout the height region (15 and 80 km). Hence, the AGWs can easily cross the critical levels when the wind direction is not changing drastically with respect to altitude, while they also pass through the critical levels when they propagate opposite to wind direction (Eckermann et al., 2007; Niranjan Kumar et al., 2012). It means that AGWs mostly coming from the east of TRGCPs can affect, and hence we observed WFs. This also suggests that the Storm 1 is the most probable source for the observed WFs on the NAA, NAU, and NML transmitter signals. The observation of stronger WFs at NML compared to NAU and their almost same time appearance at both signals can also be understood in terms of background wind direction. As can be seen from Figure 1c, the background wind direction is slightly southeast; hence, southward propagation of AGWs might have been affected/slowed down (Nishioka et al., 2013). Further, AGWs from Storm 2 would mostly be propagating southward (as background wind direction at 80 km is toward north), and hence minimal effect could be seen on the NPM signals. In nutshell we have verified the possibilities for the observed WFs, and the observations suggest that the most probable source for the WFs is the convective Storm 1 for most of the TRGCPs except for NPM, where the observed disturbances may probably be caused by Storm 2. This indicates that the background wind significantly affects propagation of AGWs. *Nishioka et al.*[2013] also discussed important role of background wind. They have observed AGWs more clearly at the north than at the south of observation location. They have suggested that when background wind velocity is comparable to the AGWs and toward southward, this restricts AGWs to propagate southward. Here, it should be noted that ionospheric observations of AGWs depend on the several parameters such as convective activity, storm intensity (lightning activity), ionospheric plasma density, recombination, and geomagnetic filed, apart from background wind (Georges, 1973; Nishioka et al., 2013; Prasad et al., 1975). With limited data set, it is difficult to determine the role of plasma density and recombination and its effect on AGWs propagation. The presence of geomagnetic field causes an anisotropy in the difference in attenuation for the propagation from west to east versus east to west. Due to this, waves travelling eastward experience less attenuation than waves travelling westward (Wait & Spies, 1964). This difference decreases with increase in wave frequency, at ~1–4 kHz the attenuation is ~45 dB/1000 km, whereas at ~20 kHz, the difference is only 1 dB/1000 km (Wait & Spies, 1964). In present case, all transmitters have frequency higher than 20 kHz (see Table 1); therefore, geomagnetic field effect may not be very significant. This is also clear by the magnitude of observed amplitude of both DHO and NPM at PARI (see Figure 2a, amplitude level is same for both).

Further in order to understand the AGWs propagation and coupling mechanism from troposphere to ionosphere, we have analyzed temperature profile from COSMIC satellite. The temperature profile uses COSMIC occultation data which is obtained by the bending angle of electromagnetic waves generated by the GPS constellation satellites that are detected by the low earth orbiting satellites. For more details on this, please see paper by Feltz et al. (2017). The data may be obtained from the following link

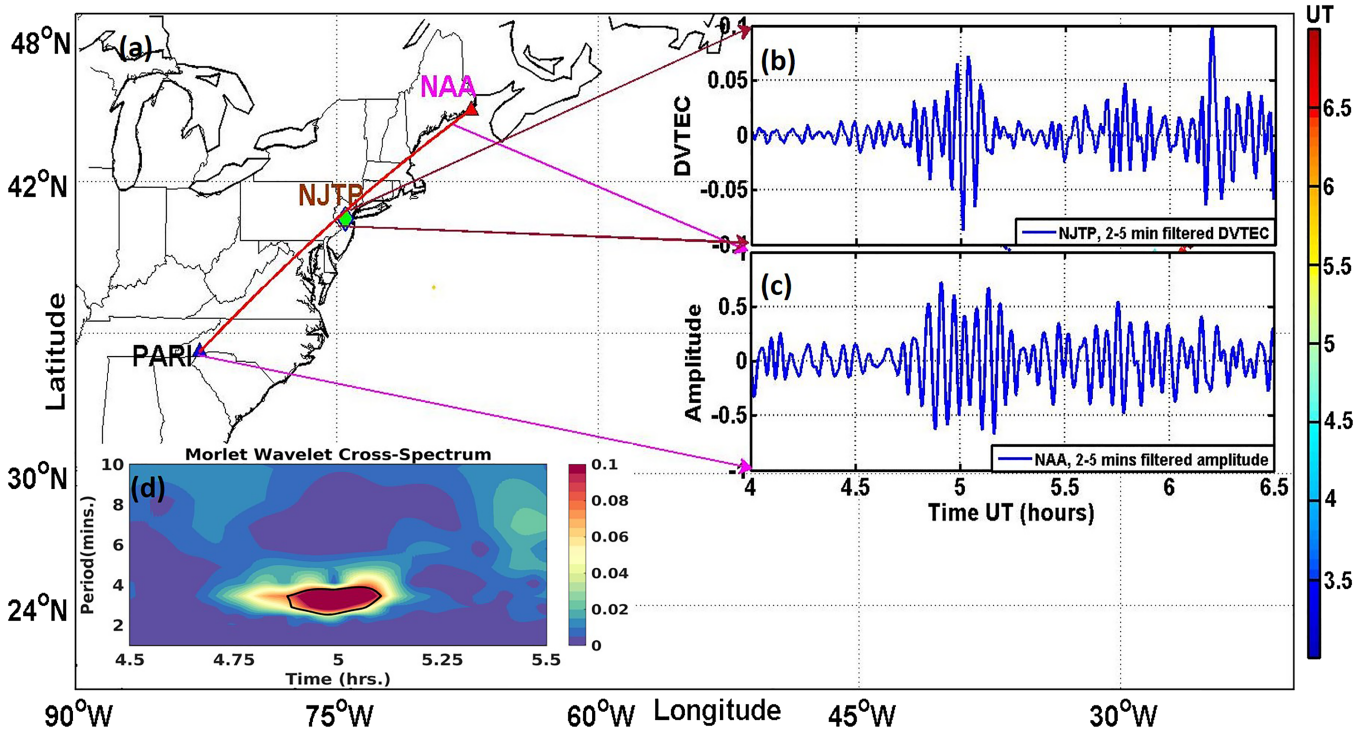

Figure 5. **(a)** Depicting the locations of NAA very low frequency (VLF) transmitter, Pisgah Astronomical Research Institute VLF receiving station and NJTP GPS station along with lightning activity during 3–7 Universal Time. **(b)** Show the 2–5 min filtered amplitude of filtered differential vertical total electron content for the NJTP GSP station. **(c)** Similar 2–5 min filtered amplitude of NAA VLF signal also shown. **(d)** Shows the time versus periodicity map of cross-wavelet power between the two signals.

(https://cdaac-www.cosmic.ucar.edu/). Figure 5a shows the COSMIC temperature profile close to PARI station up to 40-km altitude. Though we can get some model data until MLT region, we can't see such fine-scale structures as the model vertical resolution is very poor when compared to the COSMIC.

Temperature profile gives information regarding the modulation due to vertically propagating gravity waves. As in the present case, the probable source is the thunderstorm; therefore, AGWs might be propagating above the troposphere. In order to confirm propagation of AGWs from below, we performed the wavelet analysis spatially (in vertical direction) to see the fluctuations in the temperature profile (Figure 5b). As can be seen from Figure 6b, the strong WFs are present. Assuming these are generated from the convection below, we obtained the vertical wavelength of the wave of 4–6 km, which is highly monochromatic and is observed throughout the troposphere and stratosphere and therefore strengthen our results that the short period gravity waves generated from the below propagated into the lower ionosphere.

It is surmised that the generated AGWs from strong convective zone must propagate with very low attenuations to travel such a long distances reaching TRGCPs at different locations. As suggested by Fritts and Alexander (2003), AGWs can propagate larger distances in the ducted mode, and hence it might be possible that AGWs from this convective zone may have propagated toward west all the way from its location. Francis (1975) was the first to theoretically describe the possibility of thermospheric duct, from where leaking of atmospheric waves takes place at ~80-km altitude. Atmospheric waves released from the supercell can be trapped in a thermal duct in the mesosphere and/or thermosphere. The altitude of the thermal duct depends on the horizontal wavelength and periods of the atmospheric waves. The altitude of the duct can also be around 80 km (Snively et al., 2010). There is also a report that some of the ducted wave energy could leak into the upper thermosphere and excite gravity waves (Shinagawa et al., 2007; Snively & Pasko, 2008). The work by Isler et al. (1997) and Walterscheid et al. (2001) suggested that many of the short-period waves observed in their data sets (e.g., airglow imager data) may be guided or trapped by a Doppler or thermal duct. These ducts are formed out of wind or thermal structure and confined wave propagation to a fixed altitude. Because they are vertically confined and

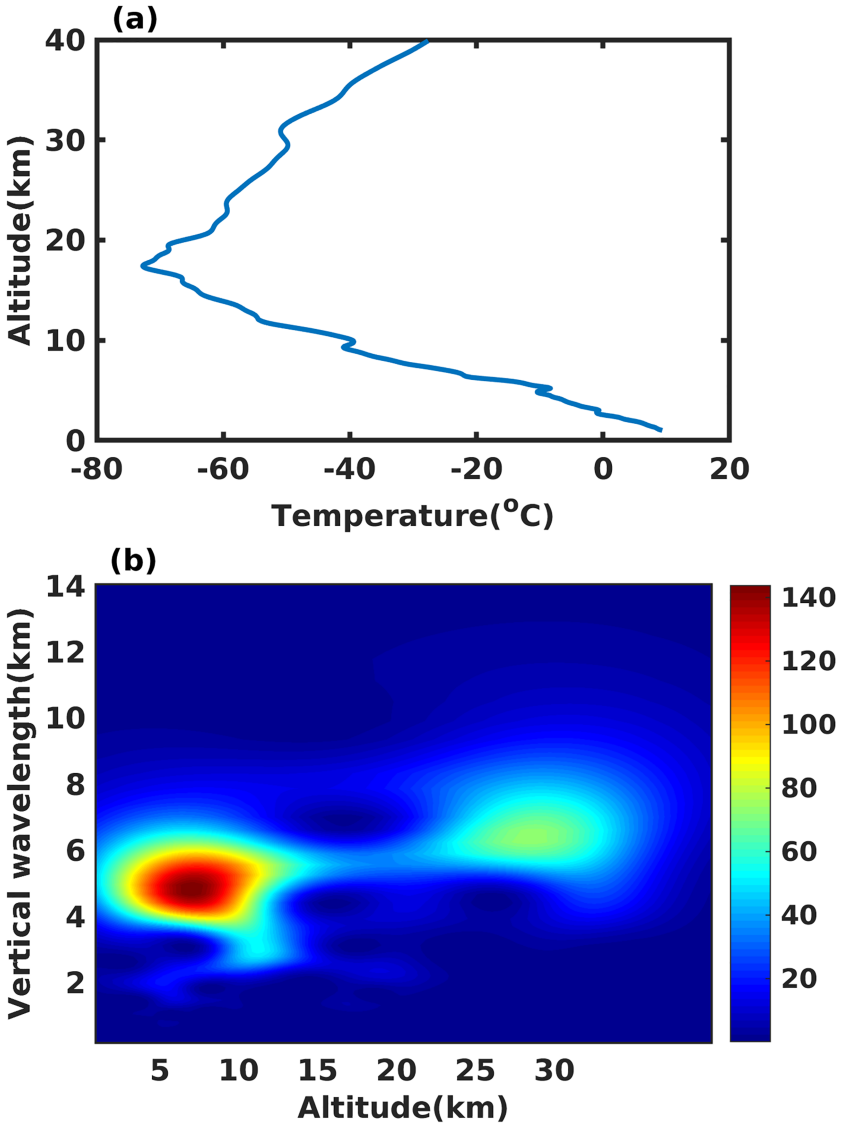

Figure 6. (a) The temperature profile obtained from the COSMIC satellite 21 January 2016 at a location (79.2°W, 31.1°N) close to the Pisgah Astronomical Research Institute receiving station. (b) The wavelet spectrum of the temperature perturbations of Figure 6a, which indicates the vertical wavelength (*y*-axis) of wavy fluctuations with respect to the altitude (*x*-axis).

exhibit relatively minimal propagation loss, ducted waves can travel great horizontal distances, as long as the atmospheric structure remains reasonably consistent. Snively et al. (2007) presented a short-period (~4.9 min) AGWs using a multiwavelength airglow image data from Bear lake observatory, Utah. They used meteor wind data and suggest that the gravity wave was most probably ducted because of the Doppler shift imposed by this wind structure created favorable conditions for Doppler ducting of the short-period wave. Recently, Silber and Price (2017) also reported observations of similar short-period (~2.5 min) acoustic WFs (~0.2 dB) in the NSY (45.9 kHz located at Sicily, Europe) transmitter signal recorded at Tel-Aviv University (Israel). They have suggested that such WFs can be produced by lightning as well as deep convective clouds. They have identified strong lightning activity over a storm located ~700 km west of NSY transmitter as the most plausible source of disturbances. Overall, the above-mentioned works suggest that the ducted waves can propagate for a long distance. This long-distance propagation of the ducted waves could explain the observation of AGWs at long distance from Storm 1. Consequently, ducted waves are able to influence regions of the atmosphere far from the source. At this moment, it is difficult to say which ducted (Doppler or thermal or both) is dominating in present case.

4.2. Vertical Coupling of Lower and Upper Ionosphere Through AGWs

In order to characterize coupling of lower and upper ionosphere through AGWs in the vertical direction, the GPS TEC data are analyzed and compared with the VLF data. As described in the section 3.2, clear WFs can be seen in the DVTEC data at several GPS stations corresponding to Storm 1 and Storm 2, and these WFs show similar periodicity (~200 sec) to that of the WFs observations in the VLF signals (Figure 4d). We further estimated and compared the 2–5-min band pass filtered signals of both DVTEC data for NJTP GPS station and NAA VLF signal amplitude as shown in the Figure 6 (left and right inset; these stations are arbitrarily chosen). The filtered signals of both the data sets show similar WFs, however, with slight differences. This is probably due to the inherent properties of two different techniques and change in the ionospheric properties in two regions. Further, the Morlet wavelet has been used for retrieving the cross-wavelet coherence between the VLF signal amplitude and the TEC data. The lower left thumbnail in Figure 6d shows the time versus periodicity map of cross-wavelet power between the two signals. The strong signal of the periods of ~2–5 mins is clearly seen associated with the high-frequency gravity waves that we discussed earlier. Thus, overall analysis suggests that the WFs observed in the lower ionosphere are also observed in the upper ionospheric altitudes implying that there is a strong dynamical coupling between the two regions through AGWs. Lay et al. (2015) in their statistical study observed ~2–4-min acoustic fluctuations at upper ionospheric heights in the U.S. Plains and which were found closely associated with thunderstorm in space and time. Walterscheid et al. (2003) have suggested the presence of duct between the ground and thermospheric temperature gradient at ~100–120-km altitude. The acoustic waves from thunderstorm are propagated through this duct and are refracted downward and also allow through to the upper ionosphere by the thermospheric temperature gradient. Francis (1975) in their theoretical study found that the acoustic waves (period <5 min) can propagate in the duct from thunderstorm to thermosphere and up to ionospheric heights. Shinagawa et al. (2007) used atmosphere-ionosphere two-dimensional nonhydrostatic compressible model and modelled sea surface perturbation due earthquakes and their effect on the upper ionosphere. They quite successfully able to produce ~4-min oscillation in the upper ionosphere, which they suggested caused by the acoustic pulse from epicenter propagating through thermospheric duct to the upper atmosphere altitude. Most of the previous works has suggested possibility of presence of duct between ground and thermosphere, through which acoustic waves from thunderstorm/tsunami propagates to ionospheric altitude. This could be the one possible mechanism for the atmosphere-ionosphere coupling process, but further modeling and simulation work is needed to better understand coupling mechanism.

5. Summary and Conclusion

The present study discussed the signatures of AGWs in the VLF signals, which manifested as WFs at the lower ionospheric altitudes. The analysis suggests that the observed AGWs are most probably generated from the convective and lightning active regions. Further, it is shown that the AGWs generated from thunderstorms propagate upward from lower ionosphere to upper ionosphere, thus contributing in the atmosphere-ionosphere coupling mechanism. Though this is a case study, nonetheless it brings out the signatures of AGWs and discuses the possible source mechanisms including their role in atmosphere-ionosphere coupling. Efforts are under way to bring out the comprehensive characteristics of AGWs and their role in ionospheric modulations by analyzing a greater number of events and through modeling efforts.

Acknowledgments
The author AKM thanks Science and Education Research Board for financial support under Ramanujan Fellowship (File No SB/S2/RJN-052/2016); the United Sates India Education Foundation (USIEF), New Delhi, India, for financial support under Fulbright-Nehru postdoctoral fellowship grant (9/1123(0001)/2 K14-485EMR-I) during which this work was initiated and Faculty Recharge Program (FRP) of University Grant Commission (UGC; ID FRP62343), New Delhi, India. The VLF data set used in the present work uploaded to a repository and can be accessed from the link (https://doi.org/10.5281/zenodo.3378264). The GOES 13 mid infrared (IR) images are taken from Dundee website (http://www.sat.dundee.ac.uk/). The source of geomagnetic conditions used is from space-weather.com website (http://www.spaceweather.com/) and WDC for Geomagnetism website (http://wdc.kugi.kyoto-u.ac.jp/). The GPS TEC measurements are obtained from several GPS receiving stations from the CORS (Continuously Operating Reference Station), available at NGS website (http://geodesy.noaa.gov/CORS/).

References

Alexander, M. J., Holton, J. R., & Durran, D. (1995). The gravity wave response above deep convection in a squall line simulation. *Journal of the Atmospheric Sciences*, *52*, 2212–2226.

Alexander, M. J., & Teitelbaum, H. (2007). Observation and analysis of a large amplitude mountain wave event over the Antarctic Peninsula. *Journal of Geophysical Research*, *112*, D21103. https://doi.org/10.1029/2006JD008368

Alexander, M. J., & Teitelbaum, H. (2011). Three-dimensional properties of Andes mountain waves observed by satellite: A case study. *Journal of Geophysical Research*, *116*, D23110. https://doi.org/10.1029/2011JD016151

Butterworth, S. (1930). On the Theory of Filter Amplifiers. *Wireless Engineer*, *7*, 536–541.

Cohen, M. B., Inan, U. S., & Paschal, E. W. (2010). Sensitive broadband ELF/VLF radio reception with the AWESOME instrument. *IEEE Transactions on Geoscience and Remote Sensing*, *48*(1), 3–17. https://doi.org/10.1109/TGRS.2009.2028334

Cohen, M. B., Said, R. K., Paschal, E. W., Mc Cormick, J. C., Gorss, N. C., Thompson, L., et al. (2018). Broadband longwave remote sensing instrumentation. *The Review of Scientific Instruments*, *89*, 094501. https://doi.org/10.1063/1.5041419

Durran, D. R. (1986). Mountain waves. In P. Ray (Ed.), *Mesoscale Meteorology and Forecasting* (pp. 472–492). Boston, Mass: Am. Meteorol. Soc.

Eckermann, S. D., Jun, M., Wu, D. L., & Broutman, D. (2007). A three- dimensional mountain wave imaged in satellite radiance throughout the stratosphere: Evidence of the effects of directional wind shear. *Quarterly Journal of the Royal Meteorological Society*, *133*, 1959–1975. https://doi.org/10.1002/qj.187

European Centre for Medium-Range Weather Forecasts (2017). updated monthly. ERA5 Reanalysis. Research Data Archive at the National Center for Atmospheric Research, Computational and Information Systems Laboratory. https://doi.org/10.5065/D6X34W69

Feltz, M. L., Knuteson, R. O., & Revercomb, H. E. (2017). Assessment of COSMIC radio occultation and AIRS hyperspectral IR sounder temperature products in the stratosphere using observed radiances. *Journal of Geophysical Research: Atmospheres*, *122*, 8593–8616. https://doi.org/10.1002/2017JD026704

Francis, S. H. (1975). Global propagation of atmospheric gravity waves: A review. *Journal of Atmospheric and Solar - Terrestrial Physics*, *37*, 1011–1064.

Fritts, D. C., & Alexander, M. J. (2003). Gravity wave dynamics and effects in the middle atmosphere. *Reviews of Geophysics*, *41*(1), L09801. https://doi.org/10.1029/2001RG000106

Garcia, R. R., & Solomon, S. (1985). The effect of breaking gravity waves on the dynamics and chemical composition of the mesosphere and lower thermosphere. *Journal of Geophysical Research*, *90*, 3850–3868.

Georges, T. M. (1973). Infrasound from convective storms: Examining the evidence. *Reviews of Geophysics and Space Physics*, *11*(3), 571–594.

Hines, C. O. (1960). Internal atmospheric gravity waves at ionospheric heights. *Canadian Journal of Physics*, *38*, 1441–1481.

Isler, J. R., Taylor, M. J., & Fritts, D. C. (1997). Observational evidence of wave ducting and evanescence in the mesosphere. *Journal of Geophysical Research*, *102*, 26,301–26,313.

John, S. R., & Kumar, K. K. (2013). A discussion on the methods of extracting gravity wave perturbations from space-based measurements. *Geophysical Research Letters*, *40*, 2406–2410. https://doi.org/10.1002/grl.50451

Jones, P. W., Hamilton, K., & Wilson, R. J. (1997). A very high resolution general circulation model simulation of the global circulation in austral winter. *Journal of the Atmospheric Sciences*, *54*, 1107–1116.

Kherani, E. A., Lognonn'e, P., Kamath, N., Cresponand, F., & Garcia, R. (2009). Response of the ionosphere to the seismic triggered acoustic waves: electron density and electromagnetic fluctuations. *Geophysical Journal International*, *176*, 1–13. https://doi.org/10.1111/j.1365-246X.2008.03818.x

Kumar, A., & Kumar, S. (2014). Space weather effects on the low latitude D region ionosphere during solar minimum. *Earth, Planets and Space*, *66*(1), 1–10. https://doi.org/10.1186/1880-5981-66-76

Kumar, K. K. (2006). VHF radar observations of convectively generated gravity waves: some new insights. *Geophysical Research Letters*, *33*, L01815. https://doi.org/10.1029/2005GL024109

Kuo, C. L., & Lee, L. C. (2015). Ionospheric plasma dynamics and instability caused by upward currents above thunderstorms. *Journal of Geophysical Research: Space Physics*, *120*, 3240–3253. https://doi.org/10.1002/2014JA020767

Lay, E. H., Shao, X. -M., & Carrano, C. S. (2013). Variation in total electron content above large thunderstorms. *Geophysical Research Letters*, *40*, 1945–1949. https://doi.org/10.1002/grl.50499

Lay, E. H., Shao, X.-M., Kendrick, A. K., & Carrano, C. S. (2015). Ionospheric acoustic and gravity waves associated with midlatitude thunderstorms. *Journal of Geophysical Research: Space Physics*, *120*, 6010–6020. https://doi.org/10.1002/2015JA021334

Malardel, S., Wedi, N., Deconinck, W., Diamantakis, M., Kuhnlein, C., Mozdzynski, G., et al., (2015). A new grid for the IFS. Newsletter No. *146* - Winter 2015/16, ECMWF, 6.

Marshall, R. A., & Snively, J. B. (2014). Very low frequency sub ionospheric remote sensing of thunderstorm-driven acoustic waves in the lower ionosphere. *Journal of Geophysical Research: Atmospheres*, *119*, 5037–5045. https://doi.org/10.1002/2014JD021594

Matsumura, M., Shinagawa, H., & Iyemori, T. (2012). Horizontal extension of acoustic resonance between the ground and the lower thermosphere. *Journal of Atmospheric and Solar - Terrestrial Physics*, *75-76*, 127–132. https://doi.org/10.1016/j.jastp.2011.12.003

Maurya, A. K., Phanikumar, D. V., Singh, R., Kumar, S., Veenadhari, B., Kwak, Y.-S., et al. (2014). Low-mid latitude D region ionospheric perturbations associated with 22 July 2009 total solar eclipse: Wave-like signatures inferred from VLF observations. *Journal of Geophysical Research: Space Physics*, *119*, 8512–8523. https://doi.org/10.1002/2013JA019521

Maurya, A. K., Veenadhari, B., Singh, R., Kumar, S., Cohen, M. B., Selvakumaran, R., et al. (2012a). Morphological features of tweeks and nighttime D region ionosphere at tweek reflection height from the observations in the low-latitude Indian sector. *Journal of Geophysical Research*, *117*(A5), A05301. https://doi.org/10.1029/2011JA016976

Maurya, A. K., Veenadhari, B., Singh, R., Kumar, S., Cohen, M. B., Selvakumaran, R., et al. (2012b). Nighttime D region electron density measurements from ELF-VLF tweek radio atmospherics recorded at low latitudes. *Journal of Geophysical Research*, *117*(A11), A11308. https://doi.org/10.1029/2012JA017876

Miller, S. D., Straka, W. C. III, Yue, J., Smith, S. M., Alexander, M. J., Hoffmann, L., et al. (2015). Upper atmospheric gravity wave details revealed in nightglow satellite imagery. *Proceedings of the National Academy of Sciences*, *112*(49), E6728–E6735. https://doi.org/10.1073/pnas.1508084112

Nina, A., & Čadež, V. M. (2013). Detection of acoustic-gravity waves in lower ionosphere by VLF radio waves. *Geophysical Research Letters*, *40*, 4803–4807. https://doi.org/10.1002/grl.50931

Niranjan Kumar, K., Ramkumar, T. K., & Krishnaiah, M. (2012). Analysis of large-amplitude stratospheric mountain wave event observed from the AIRS and MLS sounders over the western Himalayan region. *Journal of Geophysical Research*, *117*, D22102. https://doi.org/10.1029/2011JD017410

Nishioka, M., Tsugawa, T., Kubota, M., & Ishii, M. (2013). Concentric waves and short period oscillations observed in the ionosphere after the 2013 Moore ef5 tornado. *Geophysical Research Letters*, *40*, 5581–5586. https://doi.org/10.1002/2013GL057963

Ozeki, M., & Heki, K. (2010). Ionospheric holes made by ballistic missiles from North Korea detected with a Japanese dense GPS array. *Journal of Geophysical Research*, *115*, A09314. https://doi.org/10.1029/2010JA015531

Peter, W. B., Chevalier, M. W., & Inan, U. S. (2006). Perturbations of mid-latitude sub-ionospheric VLF signals associated with lower ionospheric disturbances during major geomagnetic storms. *Journal of Geophysical Research*, *111*, A03301. https://doi.org/10.1029/2005JA011346

Piani, C., Durran, D., Alexander, M. J., & Holton, J. R. (2000). A numerical study of three-dimensional gravity waves triggered by deep tropical convection and their role in the dynamics of the QBO. *Journal of the Atmospheric Sciences*, *57*(22), 3689–3702.

Prasad, S. S., Schneck, L. J., & Davies, K. (1975). Ionospheric disturbances by severe tropospheric weather storms. *Journal of Atmospheric and Terrestrial Physics*, *37*, 1357–1363.

RamaRao, P. V. S., Gopikrishna, S., Niranjan, K., & Prasad, D. S. V. V. D. (2006). Temporal and spatial variations in TEC using simultaneous measurements from the Indian GPS network of receivers during the low solar activity period of 2004–2005. *Annales de Geophysique*, *24*, 3279–3292.

Said, R. K., Cohen, M. B., & Inan, U. S. (2013). Highly Intense Lightning Over the Oceans: Estimated Peak Currents from Global GLD360 Observations. *Journal of Geophysical Research: Atmospheres*, *118*, 6905–6915. https://doi.org/10.1002/jgrd.50508

Said, R. K., Inan, U. S., & Cummins, K. L. (2010). Long range lightning geolocation using a VLF radio atmospheric waveform bank. *Journal of Geophysical Research*, *115*, D23108. https://doi.org/10.1029/2010JD013863

Seemala, G. K., & Valladares, C. E. (2011). Statistics of total electron content depletions observed over the South American continent for the year 2008. *Radio Science*, *46*, RS5019. https://doi.org/10.1029/2011RS004722

Sentman, D. D., Wescott, E. M., Picard, R. H., Winick, J. R., Stenbaek-Nielsen, H. C., Dewan, E. M., et al. (2003). Simultaneous observations of mesospheric gravity waves and sprites generated by a midwestern thunderstorm. *Journal of Atmospheric and Terrestrial Physics*, *65* (2003), 537–550.

Shinagawa, H., Iyemori, T., Saito, S., & Maruyama, T. (2007). A numerical simulation of ionospheric and atmospheric variations associated with the Sumatra earthquake on December 26, 2004. *Earth, Planets and Space*, *59*, 1015–1026.

Silber, I., & Price, C. (2017). On the use of VLF narrowband measurements to study the lower ionosphere and the mesosphere–lower thermosphere. *Surveys in Geophysics*, *38*(2), 407–441. https://doi.org/10.1007/s10712-016-9396-9

Sinvely, J. B. (2017). Nonlinear gravity wave forcing as a source of acoustic waves in the mesosphere, thermosphere, and ionosphere. *Journal of Geophysical Research: Space Physics*, *44*, 12,020–12,027. https://doi.org/10.1002/2017GL075360

Snively, J. B. (2013). Mesospheric hydroxyl airglow signatures of acoustic and gravity waves generated by transient tropospheric forcing. *Geophysical Research Letters*, *40*, 1–5. https://doi.org/10.1002/grl.50886

Snively, J. B., & Pasko, V. P. (2008). Excitation of ducted gravity waves in the lower thermosphere by tropospheric sources. *Journal of Geophysical Research*, *113*, A06303. https://doi.org/10.1029/2007JA012693

Snively, J. B., Pasko, V. P., & Taylor, M. J. (2010). OH and OI airglow layer modulation by ducted short-period gravity waves: Effects of trapping altitude. *Journal of Geophysical Research*, *115*, A11311. https://doi.org/10.1029/2009JA015236

Snively, J. B., Pasko, V. P., Taylor, M. J., & Hocking, W. K. (2007). Doppler ducting of short-period gravity waves by midlatitude tidal wind structure. *Journal of Geophysical Research*, *112*, A03304. https://doi.org/10.1029/2006JA011895

Vadas, S. L. (2013). Compressible f-plane solutions to body forces, heatings, and coolings, and application to the primary and secondary gravity waves generated by a deep convective plume. *Journal of Geophysical Research: Space Physics*, *118*, 1–21. https://doi.org/10.1002/jgra.50163

Vadas, S. L., & Liu, H. L. (2009). Generation of large-scale gravity waves and neutral winds in the thermosphere from the dissipation of convectively generated gravity waves. *Journal of Geophysical Research*, *114*, A10310. https://doi.org/10.1029/2009JA014108

Wait, J. R., & Spies, K. P. (1964). Characteristics of the earth-ionosphere waveguide for VLF radio waves, *Tech. Note 300, Natl. Bur. of Stand.*, Boulder, Co.

Walterscheid, R. L., Schubert, G., & Brinkman, D. G. (2001). Small-scale gravity waves in the upper mesosphere and lower thermosphere generated by deep tropical convection. *Journal of Geophysical Research*, *106*, 31,825–31,832.

Walterscheid, R. L., Schubert, G., & Brinkman, D. G. (2003). Acoustic waves in the upper mesosphere and lower thermosphere generated by deep tropical convection. *Journal of Geophysical Research*, *108*(A11), 1392. https://doi.org/10.1029/2003JA010065